Kinetics of Mesophase Transitions in Thermotropic Copolyesters. 5. A Copolyester Containing TPA/PHQ/HBA

Ronald L. Johnson and Stephen Z. D. Cheng*

Institute and Department of Polymer Science, College of Polymer Science and Polymer Engineering, University of Akron, Akron, Ohio 44325-3909

Received July 6, 1992; Revised Manuscript Received October 8, 1992

ABSTRACT: The copolyester consisting of 90 mol % phenylhydroquinone terephthalate (TPA/PHQ) and 10 mol % hydroxybenzoic acid (HBA) has been studied by differential scanning calorimetry (DSC), wide-angle X-ray diffraction (WAXD), and polarized light microscopy (PLM). Upon cooling from the liquid crystal phase, two exothermic processes are observed. Neither of these processes can be by-passed when the sample is quenched. Results from nonisothermal DSC studies demonstrate that the exotherm occurring at higher temperatures corresponds to a nematic phase transition, and this transition is monotropic. The exotherm occurring at lower temperatures corresponds to a mesophase transition, resulting in a packing close to pseudohexagonal. Crystallization can take place using prolonged annealing times. Two kinds of crystals with different stabilities can be formed depending upon crystallization conditions. WAXD fiber patterns show that the crystals formed are monoclinic. Isothermal DSC experiments illustrate that the annealing kinetics at different temperatures are characterized by fractional Avrami exponents. Heat capacity data provide evidence that the glass transition temperature of TPA/PHQ/HBA (45/45/10) is around 460 ± 10 K. The changes of the glass transition and crystal melting behavior are dependent on different thermal histories. The effect of the crystal on the interfacial structure is also discussed.

Introduction

Thermotropic aromatic copolyesters are of commercial interest due to their ability to form anisotropic melts which yield good injection-molding properties and their ability to form fibers, films, and coatings. They are also of interest academically since they provide an opportunity to study how chain rigidity and structure regularity affect the molecular order and motion in polymeric materials.

High molecular weight poly(oxy-1,4-phenylenecarbonyl) (HBA) was first described by Economy et al.[1-4] This polymer is highly crystalline and forms two crystal phases (I and II) at room temperature based on electron diffraction patterns.[5,6] Both of the polymorphs are orthorhombic, and they partially transform at around 623 K into a pseudohexagonal polymorph III.[5] This transformation is reversible. The phase III has a density which is 11% lower than the polymorphs I and II.[5] Experimental observations of this transition at 623 K have been reported based on differential scanning calorimetry (DSC), and wide-angle X-ray diffraction (WAXD) methods.[1-8] This form has variously been described as a plastic crystal,[2] a highly ordered smectic liquid crystal,[2,9] and a conformationally disordered crystal.[10] However, the isotropization temperature of this polymer is very high so that decomposition occurs before realization of the melt state.[11] To lower the transition temperatures of this thermotropic aromatic copolyester, the packing of the chains in the crystalline state must be disrupted. This may be accomplished by disrupting the chain packing along the backbone or in the direction lateral to the chain backbone.[12]

One example is the copolymer of para (p) and meta (m) isomers of HBA. A 95/5 p-m copolyester shows a transition of the phase III to the isotropic melt at 653 K.[7,13] Poly(oxy-1,4-phenylenecarbonyl-*co*-oxy-2,6-naphthoyl) (HBA/HNA) is another example of packing being disrupted along the chain backbone. This system shows poor crystallinity as compared to the crystals of the HBA homopolymer. Two transition processes have been found to occur when cooling from the liquid crystal state:[14-16] a fast transition process during quenching results in a pseudohexagonal packing, and a slow transition process during annealing results in an orthorhombic packing. WAXD studies of drawn fibers have shown aperiodicity along the meridional layers. Blackwell has proposed a model using limited matching along meridional layers,[17,18] while Windle has suggested a model based on the matching of co-units.[19] Computer modeling has provided a unique method to explain the WAXD patterns.[17-20] A range of compositions has been studied and the results summarized in terms of a phase diagram.[21,22]

An example of lowering transition temperatures by disrupting the lateral packing of the chains is the copolyesters consisting of terephthalic acid, phenylhydroquinone, and (1-phenylethyl)hydroquinone (TPA/PHQ/PEHQ).[23-25] Crystals formed during both processes are monoclinic. A phase diagram was constructed based on nonisothermal DSC scans and results from WAXD fiber studies. The system shows solid solution behavior. Modeling of the WAXD fiber patterns was also carried out.[26]

The purpose of this study is to concentrate on a copolyester consisting of 90 mol % phenylhydroquinone terephthalate and 10 mol % HBA. The chemical structure is

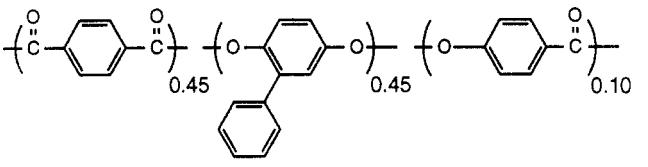

The area of interest is to identify how the addition of HBA units affects the mesophase and glass transition behavior and the ordered structure of TPA/PHQ copolyesters.

Experimental Section

Materials and Samples. The copolyester consisting of terephthalic acid (TPA), phenylhydroquinone (PHQ), and hydroxybenzoic acid (HBA) was provided by the Du Pont Co. through the International Union of Pure and Applied Chemistry (IUPAC) Working Party on Polymeric Liquid Crystals. The composition obtained consisted of TPA/PHQ/HBA in relative mole percentages of 45/45/10. The statistical molecular mass of the repeat unit is 296.7 g/mol. The as-received material was cut

0024-9297/93/2226-0094$04.00/0

into pieces of approximately 1 mm on a side. The molecular mass of this material was increased by solid-state polymerization under nitrogen at 550 K for 24 h.

For DSC studies the dried sample was placed into DSC pans which were then hermetically sealed. To avoid the effect of previous thermal history, each sample was used only once. The sample weights were between 10 and 15 mg. Empty pans were weighed to match within a deviation of ±0.005 mg.

Melt-drawn fibers were used to determine the unit cells. The diameter of a single fiber was about 1 denier. Bundles of ~50 fibers were prepared. Annealing was performed on separate bundles at 495 and 535 K in a nitrogen atmosphere at fixed length, and then the bundles were cooled to room temperature very slowly (about 1–2 K/min).

Samples used for the powder patterns were prepared by pressing the amount of copolyester necessary to form a film with dimensions of 2.5 × 2.0 × 0.05 cm^3.

Differential Scanning Calorimetry (DSC). Experiments were performed on a Perkin-Elmer DSC-2 and a Du Pont 910 DSC coupled with a 9900 Thermal Analysis System. Calibration of temperature was conducted using a set of standard materials. The instruments were also calibrated at different heating rates using an indium standard. A sapphire single crystal was used as the reference for the heat capacity studies.

In the nonisothermal experiments, the sample was heated to 30 K above the disordering temperature and held at this temperature for 1.5 min. The samples were then cooled to room temperature at different rates and were subsequently heated at a rate of 10 K/min unless otherwise noted. The onset temperature was taken on the high-temperature side of the traces during cooling and on the low temperature side of the traces during heating. The isothermal DSC experiments were conducted by initially heating the sample to a temperature 30 K above the disordering temperature. The samples were then cooled at 320 K/min to a predetermined temperature. After the desired isothermal time was achieved, the samples were heated at a rate of 10 K/min.

The glass transition temperature was taken as the temperature at 50% vitrification as determined by the heat capacity change during the transition.

Wide-Angle X-ray Diffraction (WAXD). Experiments were performed using Rigaku X-ray generators. For the powder patterns, a Model RU200 D/MAX B was used which has a 12-kW rotating anode as the source of the incident X-ray beam. For the fiber patterns, a Geigerflex model was used. A graphite crystal was used to monochromatize the beams.

The powder patterns were recorded on a pulse-height analyzer connected to an IBM PS-2 computer in a 2θ range between 3° and 40°. The fiber patterns were taken in a vacuum camera and recorded on X-ray photofilms. Calibration of the sample-to-film distance was accomplished by coating the fibers with 325-mesh silicon powder. Several exposure times were used to allow accurate determination of the positions of both weak and strong diffraction spots. To determine a crystal unit cell, the starting point was a triangle net along ($hk0$) planes based on the reciprocal lattice. All the diffraction spots along the equatorial must fit into this net. The c-axis was determined through the layer diffraction along the meridional direction. Computer refinement was carried out in order to achieve the most precise fit of the crystal unit cell.

Isothermal experiments were conducted on samples that were heated to the liquid crystal state and then quenched to the isothermal temperature on the diffractometer. The same thermal histories were applied as in the case of the DSC measurements. Only diffraction angle changes over time were considered at each isothermal temperature.

Polarized Light Microscopy (PLM). A Nikon Labophot-pol microscope equipped with a 35-mm camera coupled to a Mettler FP-52 hot stage was used. Nonisothermal experiments consisted of placing the slide in the microscope hot stage and then heating/cooling the samples at a rate of 10 K/min. Isothermal experiments followed the same procedure as in the cases of DSC and WAXD measurements.

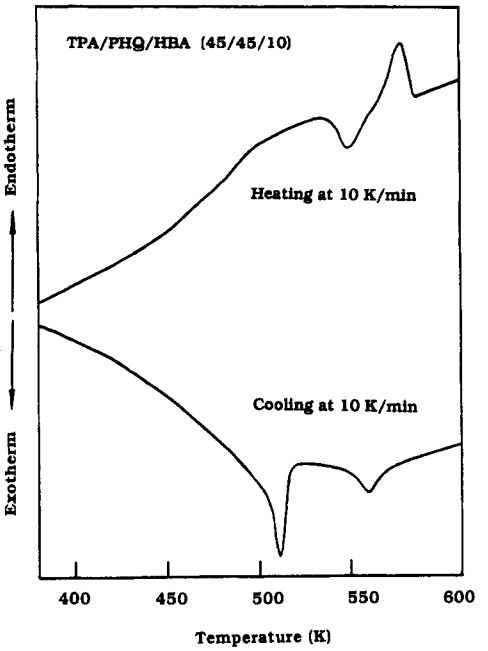

Figure 1. DSC traces of TPA/PHQ/HBA taken during heating and cooling at a rate of 10 K/min.

Table I
Onset Temperatures and Heats of Transitions for Exothermic Processes Observed on Cooling

cooling rate (K/min)	first peak		second peak	
	T (K)	ΔH (kJ/mol)	T (K)	ΔH (kJ/mol)
5	571	0.45	522	1.70
10	571	0.44	516	1.49
20	571	0.42	514	1.47
40	571	0.45	512	1.38
80	572	0.44	510	0.99

Results

Nonisothermal DSC Studies. DSC traces obtained when the TPA/PHQ/HBA copolyester is heated and cooled at a rate of 10 K/min are shown in Figure 1. The heating curve shows a single glass transition occurs over the range of 390–470 K (see below). A broad endothermic region follows that covers the temperature range of about 470–535 K with a heat of transition of 2.06 kJ/mol. Next an exothermic process is observed having a peak temperature of 553 K and an apparent heat of transition of 0.22 kJ/mol due to its overlap with the previous endothermic peak. An endothermic process (crystal melting, see below) follows which has a peak temperature of 580 K and a heat of transition of 1.14 kJ/mol. A nematic liquid crystal phase is reached (see below), and no further transitions are observed up to the decomposition temperature. When the sample is cooled at 10 K/min, two exothermic processes are observed. The first process (nematic transition, see below) has an onset temperature of 571 K and a heat of transition of 0.45 kJ/mol. The second (mesophase transition, see below) has an onset temperature of 520 K, a peak temperature of 511 K, and a heat of transition of 1.49 kJ/mol. When the polymer is cooled at rates varying from 5 to 80 K/min, the onset temperature and the heat of transition of the high temperature exothermic process remain constant at 571 K and 0.45 kJ/mol, respectively. However, the onset and peak temperatures and heat of transition of the low-temperature exothermic process decrease as the cooling rate is increased. The onset temperatures and heats of transition as a function of cooling rate for both processes are given in Table I. When the polymer is heated at rates varying from 5 to 80 K/min,

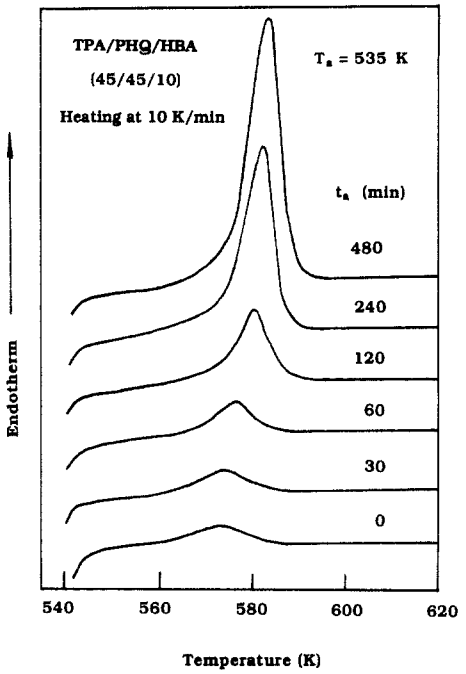

Figure 2. Set of DSC heating traces of TPA/PHQ/HBA after isothermal crystallization at T_a = 535 K for different times.

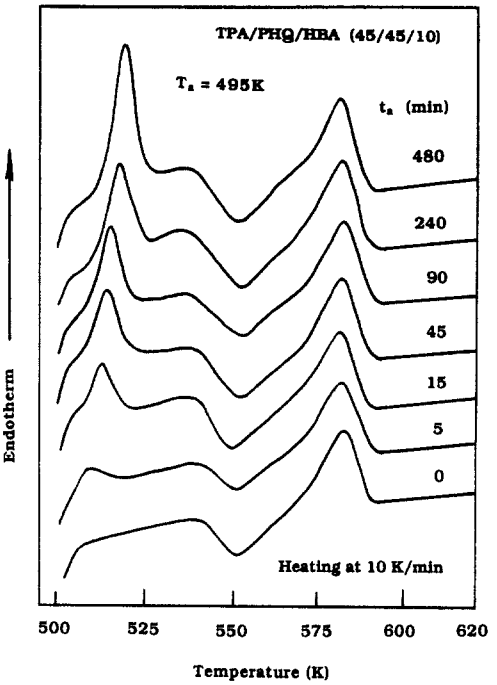

Figure 3. Set of DSC heating traces of TPA/PHQ/HBA after isothermal crystallization at T_a = 495 K for different times.

the basic shape of the heating trace is unchanged from that shown in Figure 1. When the sample is cooled from 610 to 535 K at a rate of 10 K/min and then immediately heated at 10 K/min, an endothermic peak with an onset temperature of 571 K and heat of transition of 0.45 kJ/mol which are the same respective values as those found on cooling, is observed. This transition thus shows very little supercooling effect.

Isothermal DSC Studies. Two temperatures and one temperature region were chosen for isothermal studies based on the behavior of the polymer during cooling. The first temperature was at 535 K which is between the two exothermic processes observed on cooling. As the isothermal time of the sample held at 535 K increases, the peak temperature and heat of transition increase. Representative traces are shown in Figure 2. Applying the Avrami treatment to the heat of transition data yields a dimensionality of growth, n, of 0.49.

The second isothermal temperature studied was 495 K which is below the low-temperature exothermic process seen on cooling. A peak starts to develop about 15 K above the isothermal temperature. The peak temperature and heat of transition increases as the time is increased, as shown in Figure 3. Applying the Avrami treatment to the heat of transition data gives a dimensionality, n, of 0.23. The peak temperatures and heats of transition of the subsequent exothermic and endothermic processes remain constant over the isothermal time region studied. The data for the endothermic peak temperatures and Avrami treatment of the heats of transition at the isothermal temperatures of 495 and 535 K are shown in Figures 4 and 5.

The third study was performed in the temperature region which is close to the glass transition temperature. The polymer was held isothermally for 2 h at isothermal temperatures ranging from 400 to 480 K using 10 K increments. The endothermic peaks for the temperatures of 430–480 K are shown in Figure 6. It was found that a sudden increase in the heat of transition from 0.15 to 0.45 kJ/mol occurred between the temperatures of 450 and 460 K. Annealing behavior at 480 K is similar to that at 495 K, but with a longer annealing time.

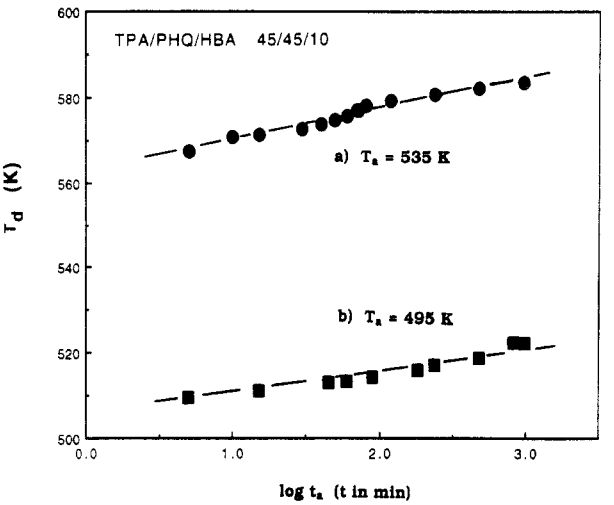

Figure 4. Relationships between transition temperatures of the melting peaks and logarithmic time at (a) T_a = 535 K and (b) T_a = 495 K.

Heat Capacity Studies. The first study was performed on a quenched sample, as shown in Figure 7. The experimental data follow the calculated solid heat capacity[27] line closely (root-mean-square (RMS) deviation of ±1%) up to a temperature of 390 K where it starts deviating. The heat capacity increases through the glass transition temperature of about 450–470 K. Instead of stopping at the liquid line, the heat capacity continues to increase. A small peak occurring at 535 K is evident, followed by a decrease showing as an exothermic peak at a temperature of 553 K. The heat capacity then increases and reaches an endothermic peak at 580 K. Above this peak, the experimental data and the calculated heat capacity in the liquid state[27] match within a RMS deviation of ±3% up to the limit of the study at 630 K. When the sample is held isothermally at 535 K for 3 h and then cooled at 1.25 K/min, Figure 8 shows that the experimentally measured heat capacity matches the calculated heat capacity in the solid state up to a temperature of 550 K, where an endothermic peak begins with a peak temperature of 562 K. A second endothermic peak is also present at 585 K.

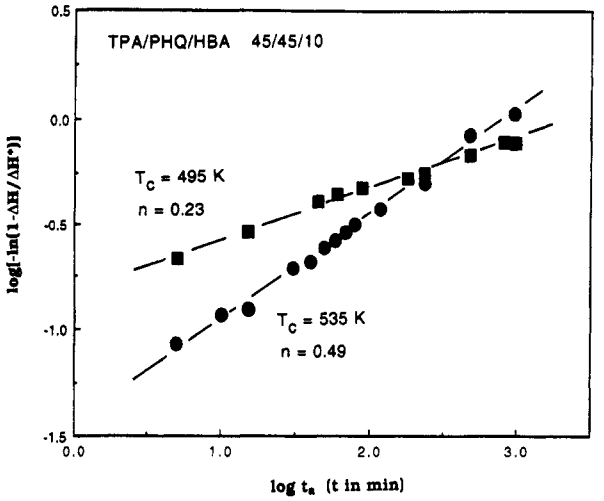

Figure 5. Avrami treatments for TPA/PHQ/HBA isothermally crystallized at two different temperatures (495 and 535 K).

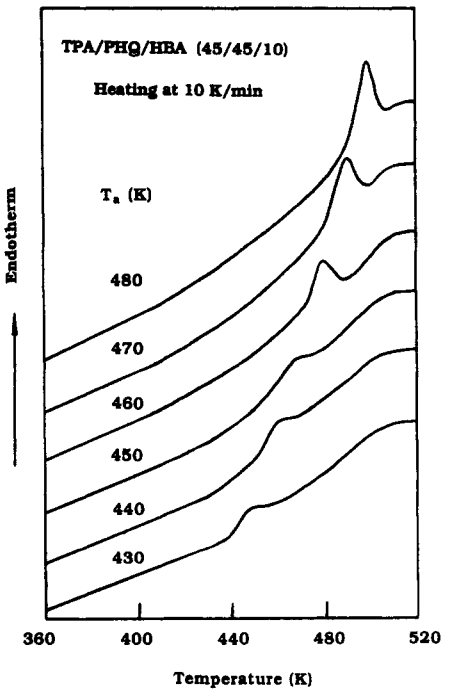

Figure 6. Set of DSC heating traces after annealing for 2 h at different temperatures.

Above this peak the experimental and calculated heat capacity data in the liquid state match closely. When the sample is held at 535 K and then quenched, Figure 9 reveals that the sample deviates from the solid heat capacity at 390 K. The heat capacity, again, increases through the glass transition temperature of 450–470 K, and a continuous increase of the heat capacity leads to a broad peak centered at 510 K. A peak subsequently follows at 585 K before the heat capacity in the liquid state is reached.

Studies were also conducted at higher annealing temperatures of 550 and 570 K. It is found that, as the magnitude of the peak observed at higher transition temperatures increases, the observed glass transition decreases.

Wide-Angle X-ray Diffraction Fiber Patterns. WAXD patterns of quenched fibers and fibers annealed at fixed lengths at temperatures of 495 and 535 K are shown in Figure 10a–c. The detailed 2θ and d-spacings for observed and calculated values of the annealed fibers are given in Tables II and III.

Figure 10a represents the WAXD pattern of quenched TPA/PHQ/HBA fibers. Along the equatorial direction,

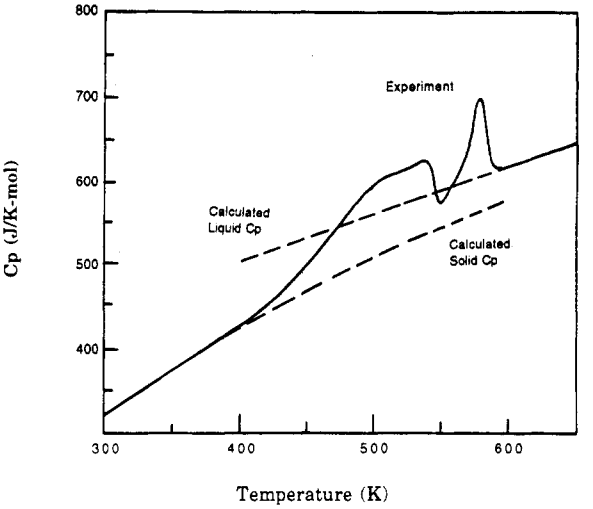

Figure 7. Heat capacity data of the quenched TPA/PHQ/HBA sample.

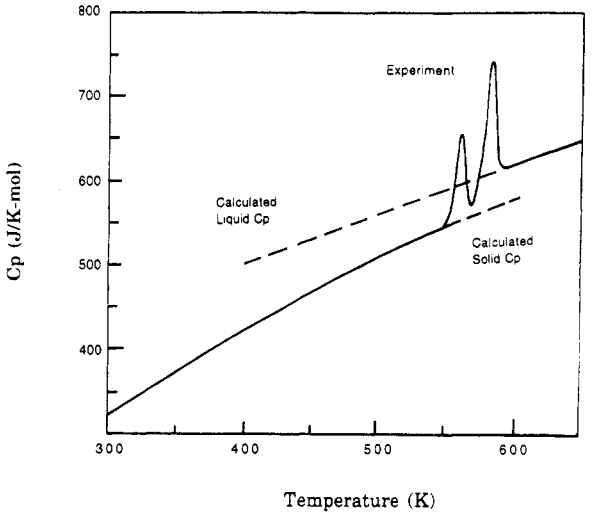

Figure 8. Heat capacity data of the sample during heating after it was annealed at 535 K for 3 h and then cooled at 1.25 K/min.

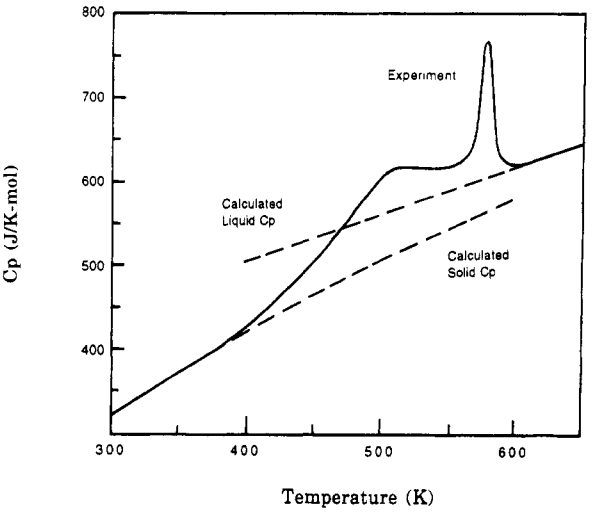

Figure 9. Heat capacity data of the sample during heating after it was annealed at 535 K for 3 h and then quenched.

only one diffuse spot can be observed in addition to a relatively low angle spot. The layer structure can, however, be seen up to 3 orders along the meridional direction. The length of the layer structure is 1.235 (±0.005) nm. The detailed unit cell cannot be determined due to the disorder of the structure perpendicular to the fiber direction. This pattern is close to a pseudohexagonal packing with an additional layer structure along the clain (fiber) direction.

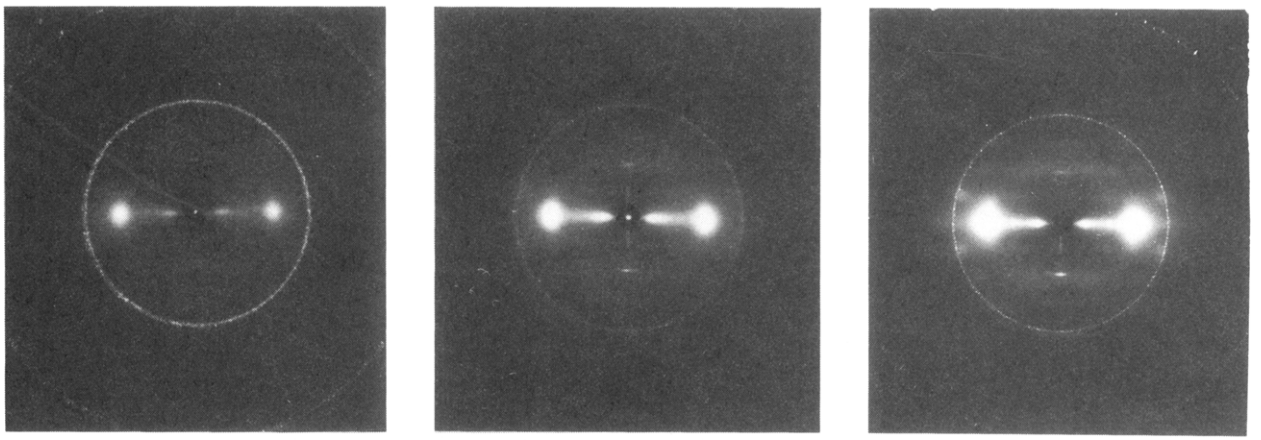

a b c

Figure 10. Wide-angle X-ray diffraction photographs of TPA/PHQ/HBA copolyester fibers: (a) quenched, (b) annealed at 495 K, (c) annealed at 535 K.

Table II
Experimental and Calculated Crystallographic Parameters of a Crystal Unit Cell for Fibers Annealed at 495 K

	2θ (deg)		d-spacing (nm)		
(*hkl*)	exptl	calcd[a]	exptl	calcd[a]	intensity[b]
(100)	6.934	6.935	1.275	1.274	s
(120)	14.33	14.37	0.6181	0.6163	m
(310)	20.19	20.01	0.4399	0.4375	vs
(001)	7.158	7.157	1.235	1.235	w
(211)	15.50	15.45	0.5717	0.5734	m
($\bar{3}$11)	25.54	25.28	0.3488	0.3524	m
(002)	14.34	14.34	0.6175	0.6175	s
(012)	16.12	16.15	0.5499	0.5487	w
(312)	24.91	24.70	0.3575	0.3604	w
(003)	21.55	21.58	0.4124	0.4177	m
(004)	28.94	28.92	0.3086	0.3088	m

[a] The calculated data listed are based on a monoclinic unit cell with a = 1.334 nm, b = 1.254 nm, c = 1.235 nm, and γ = 72.8°. [b] The intensities are semiquantitatively estimated via a microdensitometer. The intensities are classified as very strong (vs), strong (s), medium (m), and weak (w).

Table III
Experimental and Calculated Crystallographic Parameters of a Crystal Unit Cell for Fibers Annealed at 535 K

	2θ (deg)		d-spacing (nm)		
(*hkl*)	exptl	calcd[a]	exptl	calcd[a]	intensity[b]
(100)	6.950	6.949	1.272	1.272	s
(200)	13.85	13.92	0.6394	0.6360	s
(220)	16.83	17.03	0.5268	0.5205	s
($\bar{2}$30)	29.68	29.77	0.3010	0.3001	w
(310)	20.20	20.01	0.4396	0.4436	vs
(001)	7.160	7.163	1.235	1.234	w
(211)	15.29	15.45	0.5796	0.5734	m
(411)	27.52	27.74	0.3241	0.3215	m
(002)	14.34	14.35	0.6177	0.6170	s
(012)	16.19	16.16	0.5475	0.5485	w
(312)	24.95	24.71	0.3569	0.3601	w
(003)	21.51	21.60	0.4131	0.4113	m
(004)	28.93	28.94	0.3087	0.3085	m

[a] The calculated data listed are based on a monoclinic unit cell with a = 1.333 nm, b = 1.255 nm, c = 1.234 nm, and γ = 72.6°. [b] The intensities are semiquantitatively estimated via a microdensitometer. The intensities are classified as very strong (vs), strong (s), medium (m), and weak (w).

The pattern for the fibers annealed at 495 K (Figure 10b) shows three spots on the equator, three spots on the first layer line, three spots on the second layer, and one spot on each of the third and fourth layers so that a total of eleven spots were identified in this fiber pattern. The strongest diffractions were found on the equatorial and meridional directions. The diffractions on the quadrants are generally weak. The unit cell parameters were determined to be a = 1.334 (±0.003) nm, b = 1.254 (±0.003) nm, c = 1.235 (±0.003) nm, γ = 72.8° (±0.2°), and V_c = 1.974 nm^3 (see Table II). Six chains are assumed to be contained in each unit cell. The calculated crystallographic density is thus 1.50 g/cm^3.

The pattern for the fiber annealed at 535 K (Figure 10c) shows five spots on the equator, three spots on the first layer, three spots on the second layer, and one spot on each of the third and fourth layers. Thus, thirteen spots are identified. The most intense reflections are again along the equatorial and meridional directions. The (120) diffraction spot observed at the annealing temperature of 495 K is no longer seen at this annealing temperature, and two new diffraction spots of the (200) and the (220) reflections have appeared. This unit cell is also monoclinic, and the unit-cell parameters are very close (within experimental error) to the values determined for the fibers annealed at 495 K. The parameters are a = 1.333 (±0.003) nm, b = 1.255 (±0.003) nm, c = 1.234 (±0.003) nm, γ = 72.6° (±0.2°), and V_c = 1.971 nm^3 (see Table III). Six chains are, again, contained in each unit cell. The calculated crystallographic density is also 1.50 g/cm^3.

Isothermal WAXD Studies. In the WAXD powder pattern of the sample isothermally kept at 440 K, two peaks are apparent at 2θ angles of 6.81° and 19.88° (Figure 11a). These peaks remain invariant in both 2θ, peak width, and intensity when held isothermally for 10 h (Figure 11b). When the isothermal temperature is at 495 K, the same two diffraction peaks are also evident (Figure 11c; t_a = 5 min). Over the course of the isothermal period (t_a = 8 h), both of the peaks increase in their intensities and shift their positions. The peak at lower 2θ decreases from 6.75° to 6.50°, and the peak at higher 2θ increases from 19.31° to 19.40° (Figure 11d). The overall half-width of the diffraction pattern decreases from 5.32° to 5.00°. When the isothermal temperature is further increased to 550 K, the same two peaks are seen initially (Figure 11e; t_a = 10 min). They show the same trends during annealing as described for 495 K. After an isothermal period of 12 h, the peak at lower 2θ decreases from 6.70° to 6.45° and the peak at higher 2θ increases from 19.10° to 19.25° (Figure 11f). The intensities of both peaks increase, and the overall half-width of the diffraction pattern decreases from 6.77° to 6.25°. During the isothermal period, new diffraction peaks also start developing. It is particularly evident that the overall half-width of the WAXD diffraction patterns

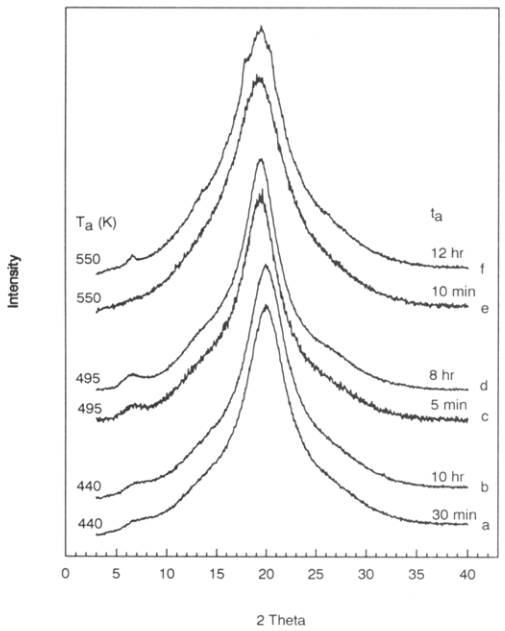

Figure 11. Wide-angle X-ray scans taken for different isothermal times at (a) T_a = 440 K, t_a = 30 min; (b) T_a = 440 K, t_a = 10 h; (c) T_a = 495 K, t_a = 5 min; (d) T_a = 495 K, t_a = 8 h; (e) T_a = 550 K, t_a = 10 min; and (f) T_a = 550 K, t_a = 12 h.

obtained at T_a = 550 K is substantially broader (about 1.5°) than those seen at lower T_as. It should be pointed out that differences among the 2θ values at different isothermal temperatures may also be caused by thermal expansion.

Polarized Light Microscopy. When the sample was observed at room temperature under crossed polarizers, it appeared highly birefringent with many small colored domains. "Threadlike" patterns are obvious. Heating and cooling of the sample up to and from a temperature of 623 K do not change its appearance and apparent morphology, but the birefringence does increase with temperature. Typical photographs of two different magnifications of the sample are shown in Figure 12.

Discussion

On the basis of the experimental observations, our discussion focuses on the transition behavior exhibited by the TPA/PHQ/HBA copolyester. What is the nature of the two exotherms observed on cooling (Figure 1)? The nonisothermal DSC experiments using different cooling rates indicate that the origins of the two peaks observed on cooling should be different. The higher temperature transition is typical of a liquid crystal transition in that the heat of transition is independent of the cooling rate and it shows little supercooling (Table I). Furthermore, immediate heating of the sample after cooling from 610 K to below 571 K gives rise to the same onset transition temperature and heat of transition, while keeping the sample isothermally below this transition leads to further crystallization (Figure 2). This reveals a typical monotropic mesophase behavior. In this case, the mesophase transition temperature is lower than the crystal melting temperature. The observation of the monotropic mesophase transition solely relies on the supercooling of the crystallization process (due to crystal nucleation) during cooling. The thermodynamics of the monotropic mesophase transition have recently been discussed in detail.[28] It has been found that many small-molecule and polymeric liquid crystal systems show this monotropic behavior.[29-32] The structure developed during this transition should not

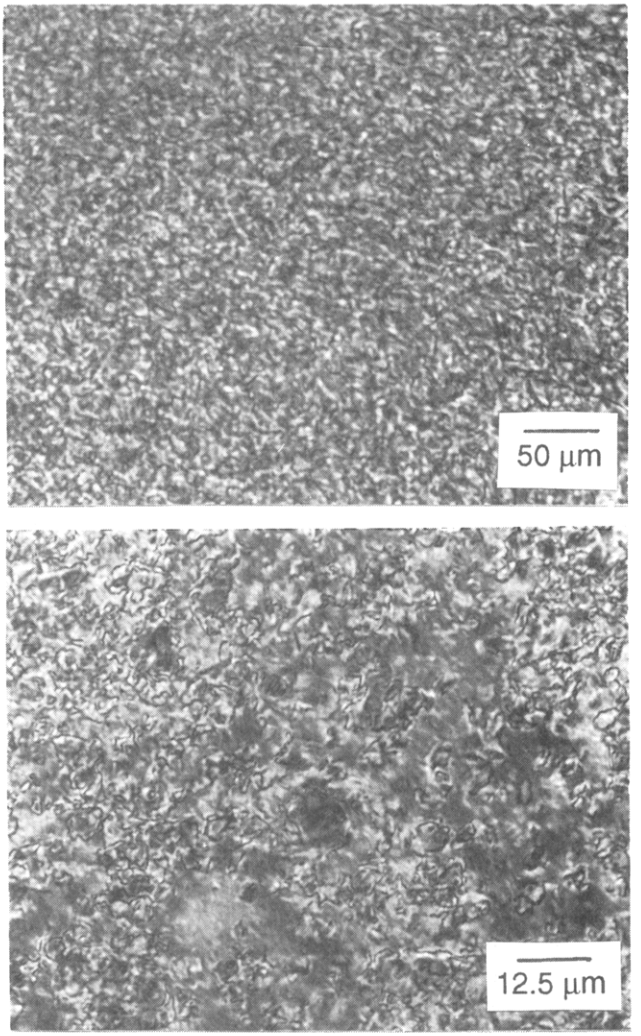

Figure 12. PLM morphological observations of TPA/PHQ/HBA with different magnifications.

be more ordered than the structure shown in Figures 10a and 11a. It may be speculated that this high-temperature monotropic transition only introduces a minor amount of order into the system since the heat and entropy changes of transition are very small (0.45 kJ/mol and 0.79 J/(K mol), respectively). Therefore, it might be a transition from a nematic I to nematic II state. Other supporting evidence is that the order of the structure developed during quenching is at most a packing close to being pseudohexagonal (see below). Furthermore, no morphological change can be observed under PLM (Figure 12) during the transitions. This indicates that the change of the morphology, if there is any, must be occurring on an even smaller scale, such as the nanometer scale.

The lower temperature transition reveals behavior typical of a crystallization or a higher ordered mesophase (such as smectic or pseudohexagonal phase) transition because it shows a decrease in both the onset temperature and heat of transition as the cooling rate is increased (Table I). This transition is thus more or less kinetically controlled. The order introduced through this lower temperature transition can be determined based on the quenched WAXD observations (Figures 10a and 11a,b). Narrowing of the half-width of the overall diffraction pattern (Figure 11) may be an indication of a (100) crystallographic plane in a packing which is close to pseudohexagonal. A lower angle diffraction peak at around 6.8–7.2° (d-spacing of about 1.2–1.3 nm) could represent either the layer structure along the chain (fiber) direction,

which corresponds to the c-axis of the crystal unit cell after the transition, or the additional diffraction peak along the equatorial direction as shown in the WAXD fiber patterns (Figure 10a–c). It should be noted that the copolyester consisting of only TPA/PHQ shows only one exothermic transition on cooling which corresponds to the fast transition process.[24] The peak temperature for this transition is 575 K, and the heat of transition is 2.7 kJ/mol. Therefore, the addition of 10 mol % HBA to the copolymer system has introduced a new nematic II transition and a new transition with a packing which is close to pseudohexagonal during cooling and which inhibited the crystallization process. To form a pseudohexagonal packing, it is necessary to have some cylindrical symmetry along the chain direction, as observed in the case of HBA/HNA.[23] Introducing HBA to the copolymer disturbs the regular chain structure and conformation of TPA/PHQ and forms defects in the crystal. However, the detailed role of 10 mol % HBA played in this copolyester is not clear at this moment and may be understood through computer modeling.

The crystal melting in TPA/PHQ/HBA is interesting because the crystal development needs prolonged crystallization time. It seems that the crystals grown at 495 K cannot be annealed to the type of crystals formed at 535 K over the isothermal time region studied. This is evidenced by the invariance of the exothermic and endothermic processes at higher temperatures after the crystals grown at 495 K melt (Figure 3). This conclusion is surprising since the crystal unit cells are almost the same for these two crystals (Figure 10b,c and Tables II and III). The change of diffraction planes must indicate a rearrangement of chain conformations in the crystal unit cells. Does this rearrangement hamper the annealing process for the low-temperature crystal to the high-temperature one? No definitive answer can be offered currently. However, direct experimental observations of the competition between the crystal growth processes of these two crystals have been found. It seems clear that the higher melting crystal cannot grow on the nuclei formed by lower melting crystals. Furthermore, better matches among the co-units may occur at higher isothermal temperatures where the mobility of the chain is greater. When better matching occurs at the higher temperatures, the chance for matching of co-units at lower temperatures decreases.

The heat capacity studies that show significant amounts of low melting crystals begin to melt at temperatures just above the glass transition. The formation of the low melting crystal is mainly due to the rapid quenching of the sample (Figures 7 and 9). The thermodynamic stability of this low melting crystal can be improved by slow cooling as shown in Figure 8. Although the overall heat of transition does not change significantly in both cases (Figures 8 and 9), the heat capacity increase at the glass transition temperature, however, behaves very differently. In Figure 8, there is practically no heat capacity increase up to 550 K. It is obviously not possible for the sample to be 100% crystalline. This behavior reveals that the noncrystalline region in the sample remains rigid until the low melting crystal is molten. It must be the case that the low melting crystal is sufficiently developed to hold the chain molecules in the noncrystalline region. This requires a strong connection of chain molecules between the crystalline and noncrystalline regions, similar to the "rigid amorphous" concept proposed several years ago as a characterization of the interfacial structure between crystalline and amorphous regions.[33,34] On the other hand, if the sample is quenched, the low melting crystal does not have the opportunity to fully develop. As a result, the less stable crystals form. When the temperature passes the glass transition temperature and the crystals start melting, they can no longer hold the chain molecules in the interfacial region and keep them rigid. In the heat capacity data shown in Figure 7, therefore, both the heat capacity increase at T_g and the crystal melting just above T_g are evident.

Due to the overlap of the glass transition region and crystal melting, it is difficult to identify the glass transition temperature. Two approaches have been tried to obtain a better estimation of the glass transition temperature. Figure 6 represents one approach. When the sample is quenched from the liquid crystalline state and subsequently annealed at different temperatures, it may exhibit two different behaviors. If the annealing temperature is below T_g, one may observe an aging phenomenon indicated by an enthalpy relaxation.[35] An endothermic process can be found in the glass transition region with a small enthalpy change of a few tenths of a kilojoule per mole, depending upon annealing temperature and time. On the other hand, if the annealing temperature is above T_g, imperfect, small crystals may grow due to the restricted chain mobility.[36] In our annealing studies, a sudden 3-fold increase in the change of enthalpy occurs between 450 and 460 K. Therefore, the glass transition temperature may lie in this region. The second approach is based on heat capacity changes. Empirically, one may expect that the heat capacity increase at T_g is about 60–70 J/(K mol) for TPA/PHQ/HBA based on the addition scheme.[37] According to the heat capacity data in the solid and liquid states, such an increase is found to be between 460 and 470 K. Both approaches have thus provided a reasonable estimation of the glass transition temperature of this copolyester, and it is around 460 ± 10 K. If one compares this value with the glass transition temperature of TPA/PHQ of 425 K,[38] it is about 35 K higher for TPA/PHQ/HBA. This might be the result of both increasing the chain rigidity and decreasing the concentration of pendent side groups through the addition of 10 mol % HBA.

The Avrami treatment for the overall crystallization process of polymeric materials has been widely used in the last 40 years. The treatment is carried out under three assumptions: (1) isothermal transition conditions, (2) random primary nucleation, and (3) linear crystal growth rate. However, these assumptions are not always valid even in the case of small-molecule crystallization processes. For oriented rigid-rod chain molecules growing longitudinally, the Avrami exponent must be around 2 if the chain molecules are fully orientated when the number of primary nuclei is constant.[39] The fractional Avrami exponents show that the material undergoes complex annealing behavior since in the transition process both pseudohexagonal and monoclinic packings are formed depending upon the isothermal time. Fractional Avrami exponents have also been reported for several transitions involving a pseudohexagonal packing in the case of HBA/HNA[15,16] and the cases of the more flexible macromolecules such as poly(tetrafluoroethylene) and *trans*-1,4-polybutadiene.[40] These fractional values may be caused by a nonnegligible nucleation volume and/or the decrease of the growth rate over time under isothermal conditions.[15,41] Nevertheless, without parallel knowledge of the microscopic morphological observations, the macroscopic, experimentally derived Avrami exponent is only a convenient means to represent empirical data of the phase transition kinetics.

It is also of interest that 10 mol % HBA leads to a change of the crystal unit-cell shape and size. From our previous studies, the crystal unit cell of TPA/PHQ is monoclinic (or pseudoorthorhombic) with the unit-cell parameters a = 1.33 nm, b = 0.91 nm, c = 1.24 nm, and γ = 90°.[24] Comparing these values with the crystal unit cell of TPA/PHQ/HBA having a = 1.33 nm, b = 1.26 nm, c = 1.24 nm, and γ = 73°, the a- and c- axes are almost unchanged, while the b-axis is expanded and γ is decreased by 17°. It has been shown that if one introduces (1-phenylethyl)-hydroquinone (PEHQ) into TPA/PHQ, more than 25 mol % is required to change the b-axis to 0.97 nm and to lower γ to less than 78°.[24] It is interesting that the introduction of HBA is more efficient in changing the crystal packing and results in a new packing which is close to pseudohexagonal. It would be interesting to study this copolyester family with changing HBA compositions to observe a systematic effect of HBA comonomers on the structure and glass transition changes.

Finally, one should point out that adding HBA may also introduce chemical transesterification at high temperatures in this copolyester, in contrast with the TPA/PHQ copolyester. This chemical process may obscure the physical transition behavior discussed here. The detailed influence of this process in this study is still unclear. Further research is awaited.

Conclusions

The addition of HBA to the TPA/PHQ system has been found to alter its transition behavior. Two exothermic processes are observed on cooling for TPA/PHQ/HBA. One of these may be a nematic phase transition which can be described as monotropic. The other is a mesophase transition forming a packing close to pseudohexagonal. Crystallization can be achieved using a prolonged annealing time. Two kinds of crystals (low and high melting) with different thermodynamic stabilities can, however, be formed depending upon the crystallization conditions. The unit cells of these crystals are both monoclinic and have the same sizes. A rearrangement of the chain conformations can be found in these two unit cells. The glass transition temperature of this copolyester has been determined to be 460 ± 10 K. When the low melting crystal is fully developed, the noncrystalline region of the polymer remains rigid until this crystal is molten, indicating strong molecular connections in the interfacial area between the crystalline and noncrystalline regions.

Acknowledgment. This work was supported by S.Z.D.C.'s Presidential Young Investigator Award from NSF (Grant DMR-9157738) and industrial matching funding provided by Exxon Education Foundation and Granmont, Inc. Their support is gratefully acknowledged.

References and Notes

(1) Economy, J.; Storm, R. S.; Matkovich, V. I.; Cottis, S. G.; Nowak, B. E. *J. Polym. Sci. Polym. Chem. Ed.* **1976**, *14*, 2207.
(2) Economy, J.; Volksen, W. In *The Strength and Stiffness of Polymers*; Zachariades, A. E., Porter, R. S., Eds.; Marcel Dekker: New York, 1983.
(3) Geiss, R.; Volksen, W.; Tsay, J.; Economy, J. *J. Polym. Sci., Polym. Lett. Ed.* **1984**, *22*, 433.
(4) Economy, J.; Volksen, W.; Viney, C.; Geiss R.; Siemens, R.; Karis, T. *Macromolecules* **1988**, *21*, 2777.
(5) Lieser, G. *J. Polym. Sci., Polym. Phys. Ed.* **1983**, *21*, 1611.
(6) Lieser, G.; Schwartz, G.; Kricheldorf, H. R. *J. Polym. Sci. Polym. Phys. Ed.* **1983**, *21*, 1599.
(7) Li, L.-S.; Lieser, G.; Rosenan-Eichlin, R.; Fischer, E. W. *Makromol. Chem., Rapid Commun.* **1987**, *29*, 159.
(8) Hanna, S.; Windle, A. H. *Polym. Commun.* **1988**, *29*, 236.
(9) Yoon, D. Y.; Masciocchi, N.; Depero, L.; Viney, C.; Parrish, W. *Macromolecules* **1990**, *23*, 1793.
(10) Wunderlich, B.; Moller, M.; Grebowicz, J.; Baur, H. *Adv. Polym. Sci.* **1988**, *87*, 1.
(11) Jackson, W. J. *Macromolecules* **1983**, *16*, 1027.
(12) Calundann, G. W.; Jaffe, M. *Robert A. Welch Conf. Chem. Res.* **1982**, *26*, 247.
(13) Rosenan-Eichlin, R.; Ballauff, M.; Grebowicz, J.; Fischer, E. W. *Polymer* **1988**, *29*, 518.
(14) Butzbach, G. D.; Wendorff, J. H.; Zimmermann, H. J. *Polymer* **1986**, *27*, 1338.
(15) Cheng, S. Z. D. *Macromolecules* **1988**, *21*, 2475.
(16) Cheng, S. Z. D.; Janimak, J. J.; Zhang, A.-Q.; Zhou, Z.-L. *Macromolecules* **1989**, *22*, 4240.
(17) Gutierrez, G. A.; Chivers, R. A.; Blackwell, J.; Stamatoff, J. B.; Yoon, H. *Polymer* **1983**, *24*, 937. See also: *Polymer Liquid Crystals*; Blumstein, A.; Ed.; Plenum: New York, 1984.
(18) Blackwell, J.; Biswas, A.; Gutierrez, G. A.; Chivers, R. A. *Faraday Discuss. Chem. Soc.* **1985**, *79*, 73.
(19) Hanna, S.; Windle, A. *Polymer* **1988**, *29*, 207.
(20) Biswas, A.; Blackwell, J. *Macromolecules* **1988**, *21*, 3146, 3152, 3168.
(21) Cao, M.-Y.; Wunderlich, B. *J. Polym. Sci., Polym. Phys. Ed.* **1985**, *23*, 521.
(22) Cao, M.-Y.; Varma-Nair, M.; Wunderlich, B. *Polym. Adv. Technol.* **1990**, *1*, 151.
(23) Cheng, S. Z. D.; Zhang, A.-Q.; Johnson, R. L.; Wu, Z.; Wu, H.-H. *Macromolecules* **1990**, *23*, 1196.
(24) Cheng, S. Z. D.; Johnson, R. L.; Wu, Z.; Wu, H.-H. *Macromolecules* **1991**, *24*, 150.
(25) Ghanem, A. M.; Dickerson, L. C.; Porter, R. S. *J. Polym. Sci., Polym. Phys. Ed.* **1990**, *28*, 1892.
(26) Hong, S.-K.; Blackwell, J. *Polymer* **1989**, *30*, 225, 780.
(27) Wunderlich, B. Report to the 1989/1990 IUPAC Working Party on Polymeric Liquid Crystals, 1991. The heat capacity in the solid state was computed based on vibrational contributions which can be separated into the skeletal vibrations (Tarasov approximation θ_1 = 528 K and θ_3 = 54 K) and the standard group vibrations. The heat capacity in the liquid state was calculated from the linear addition scheme (Cp = 268.008 + 0.588T).
(28) Percec, V.; Keller, A. *Macromolecules* **1990**, *23*, 4347.
(29) Vorlander, D. *Z. Phys. Chem.* **1923**, *105*, 211.
(30) Percec, V.; Yourd, R. *Macromolecules* **1989**, *22*, 524, 3329.
(31) Cheng, S. Z. D.; Yandrasits, M. A.; Zhang, A.-Q.; Percec, V. *Polymer* **1991**, *32*, 1284. See also: Yandrasits, M. A.; Cheng, S. Z. D.; Zhang, A.-Q.; Cheng, J.; Wunderlich, B.; Percec, V. *Macromolecules* **1992**, *25*, 2112.
(32) Pardey, R.; Zhang, A.-Q.; Gabori, P. A.; Harris, F. W.; Cheng, S. Z. D.; Lenz, R. W. *Macromolecules*, in press.
(33) Suzuki, H.; Grebowicz, J.; Wunderlich, B. *Br. Polym. J.* **1985**, *17*, 1. See also: Cheng, S. Z. D.; Cao, M.-Y.; Wunderlich, B. *Macromolecules* **1986**, *19*, 1868. Cheng, S. Z. D.; Wunderlich, B. *Macromolecules* **1987**, *20*, 1630; **1988**, *21*, 789.
(34) Cheng, S. Z. D. *J. Appl. Sci. Symp.* **1989**, *43*, 315.
(35) Berens, A. H.; Hodge, I. M. *Macromolecules* **1982**, *15*, 756.
(36) Cheng, S. Z. D.; Pan, R.; Wunderlich, B. *Makromol. Chem.* **1988**, *189*, 2443.
(37) Wunderlich, B. *J. Chem. Phys.* **1960**, *64*, 1052.
(38) Johnson, R. L. Ph.D. Dissertation, Department of Polymer Science, University of Akron, Akron, OH, 1992.
(39) Warner, S. B.; Jaffe, M. *J. Cryst. Growth* **1980**, *48*, 184.
(40) Grebowicz, J.; Cheng, S. Z. D.; Wunderlich, B. *J. Polym. Sci. Polym. Phys. Ed.* **1986**, *24*, 675.
(41) Cheng, S. Z. D.; Wunderlich, B. *Macromolecules* **1988**, *21*, 3327.